Recurring dynamically induced thinning during 1985 to 2010 on Upernavik Isstrøm, West Greenland

Shfaqat Abbas Khan,[1] Kurt H. Kjær,[2] Niels J. Korsgaard,[2] John Wahr,[3] Ian R. Joughin,[4] Lars H. Timm,[2] Jonathan L. Bamber,[5] Michiel R. van den Broeke,[6] Leigh A. Stearns,[7] Gordon S. Hamilton,[8] Bea M. Csatho,[9] Karina Nielsen,[1] Ruud Hurkmans,[5] and Greg Babonis[9]

[1] Many glaciers along the southeast and northwest coasts of Greenland have accelerated, increasing the ice sheet's contribution to global sea-level rise. In this article, we map elevation changes on Upernavik Isstrøm (UI), West Greenland, during 2003to 2009 using high-resolution ice, cloud and land elevation satellite laser altimeter data supplemented with altimeter surveys from NASA's Airborne Topographic Mapper during 2002 to 2010. To assess thinning prior to 2002, we analyze aerial photographs from 1985. We document at least two distinct periods of dynamically induced ice loss during 1985 to 2010 characterized by a rapid retreat of the calving front, increased ice speed, and lowering of the ice surface. The first period occurred before 1991, whereas the latter occurred during 2005 to 2009. Analyses of air and sea-surface temperature suggest a combination of relatively warm air and ocean water as a potential trigger for the dynamically induced ice loss. We estimate a total catchment-wide ice-mass loss of UI caused by the two events of 72.3 ± 15.8 Gt during 1985 to 2010, whereas the total melt-induced ice-mass loss during this same period is 19.8 ± 2.8 Gt. Thus, 79% of the total ice-mass loss of the UI catchment was caused by ice dynamics, indicating the importance of including dynamically induced ice loss in the total mass change budget of the Greenland ice sheet.

1. Introduction

[2] The acceleration of many of Greenland's outlet glaciers has increased the ice sheet's net contribution to global sea-level rise over the last decade [*Chen et al.*, 2006; *Khan et al.*, 2007; *Krabill et al.*, 2004; *Liu et al.*, 2012; *Rignot and Kanagaratnam*, 2006; *van den Broeke et al.*, 2009]. Several studies have shown that the increase in ice discharge from those glaciers is a consequence of significant acceleration in flow speed [*Howat et al.*, 2005; *Joughin et al.*, 2008; *Luckman et al.*, 2006; *Rignot and Kanagaratnam*, 2006; *Stearns and Hamilton*, 2007], leading to dynamically induced thinning [*Howat et al.*, 2007; *Nielsen et al.* 2012; *Pritchard et al.*, 2009]. The situation across Greenland continues to evolve. Evidence from the Gravity Recovery and Climate Experiment (GRACE) satellite gravity mission, Global Positioning System (GPS) measurements, and ice, cloud and land elevation satellite (ICESat) [*Khan et al.*, 2010; *Pritchard et al.*, 2009; *Velicogna*, 2009] suggest there is an ongoing northward migration of increasing ice loss. These observed changes in ice dynamics are likely due to climate change, yet the sensitivity of ice dynamics to climate change is not well understood or realistically included in ice-sheet models, and so its future role in global sea-level change cannot yet be predicted with much confidence [*Lemke et al.*, 2007].

[3] In this study, we estimate catchment-wide ice-mass changes on Upernavik Isstrøm (UI) from over more than a quarter century, and separate the contributions of dynamic and melt-induced ice loss. UI is located in northwest

---

[1]DTU Space–National Space Institute, Technical University of Denmark, Department of Geodesy, Kgs. Lyngby, Denmark.

[2]Centre for GeoGenetics, Natural History Museum, University of Copenhagen, Copenhagen, Denmark.

[3]Department of Physics and Cooperative Institute for Research in Environmental Sciences, University of Colorado, Boulder, Colorado, USA.

[4]Applied Physics Laboratory, University of Washington, Seattle, Washington, USA.

[5]Bristol Glaciology Centre, University of Bristol, Bristol, United Kingdom.

[6]Institute for Marine and Atmospheric Research, Utrecht University, Utrecht, the Netherlands.

[7]Department of Geology, University of Kansas, Lawrence, Kansas, USA.

[8]Climate Change Institute, University of Maine, Orono, Maine, USA.

[9]Department of Geological Sciences, University at Buffalo, Buffalo, New York, USA.

Corresponding author: S. A. Khan, Technical University of Denmark National Space Institute, Department of Geodesy, Elektrovej, Bygn. 328, 2800 Kgs. Lyngby, Denmark. (abbas@space.dtu.dk)
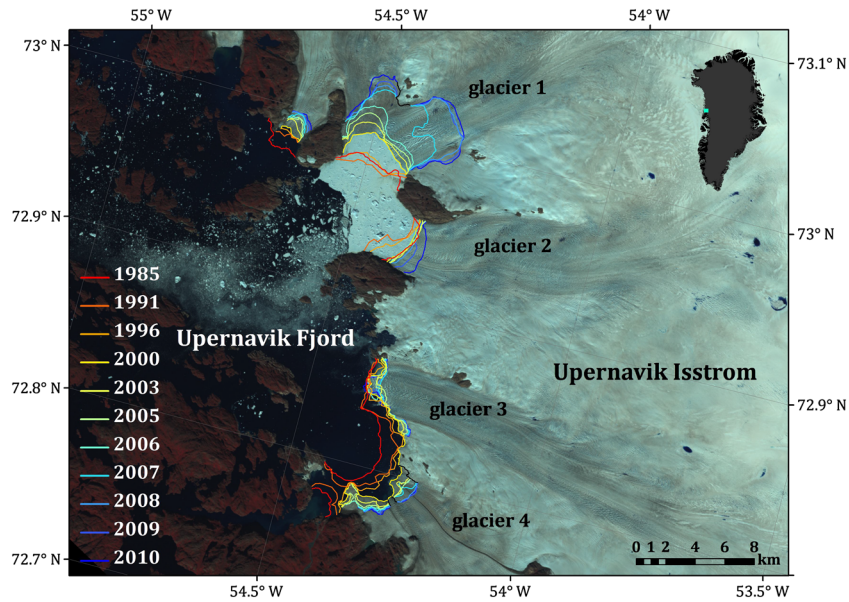
Figure 1. UI and its four main glaciers. Positions of calving fronts at various times between 1985 and 2010 are shown. The 1985 calving front is obtained from aerial photos, whereas the 1991 to 2010 fronts are based on LANDSAT images from http://glovis.usgs.gov and http://earthexplorer.usgs.gov. All images are recorded in July through August.

Greenland and consists of several outlets that we label glaciers 1 to 4 (Figure 1). We show that UI experienced at least two short-timescale accelerations in dynamically induced thinning between 1985 and 2010. The most recent acceleration started in mid-2005 (see section 3), which is consistent with other studies suggesting northward migration of increasing ice loss along the west Greenland margin starting at the same time [*Khan et al.*, 2010]. Recently, *Kjær et al.* [2012] reported dynamically induced ice-loss events on the northwestern Greenland Ice Sheet margin from 1985 to 1993 and 2005 to 2010. The first period of ice loss on UI reported in this article could possibly have taken place during 1985 to 1993.

[4] We map changes on UI during 2003 to 2009 using high-resolution ICESat laser altimeter data [*Zwally et al.*, 2010] supplemented with altimeter surveys from NASA's Airborne Topographic Mapper (ATM) flights during 2002 to 2010 [*Krabill*, 2011]. To assess thinning before 2002, we analyze 1985 aerial photos and derive a 25×25 m gridded digital elevation model (DEM).

[5] We isolate the dynamically induced thinning by comparing observed elevation changes with estimated elevation changes caused by fluctuations in surface mass balance (SMB) and firn densification, using output from the regional atmospheric climate model v.2 (RACMO2) [*van den Broeke et al.*, 2009]. SMB represents the sum of mass accumulation (snowfall, rain) and ablation (sublimation, runoff), but does not include contributions from dynamically induced thinning.

[6] Dynamically induced thinning and rapid increases in glacier ice speeds seen in many places along the Greenland and Antarctic ice margin has been attributed to decreased flow resistance and increased along-flow tensile stresses during the retreat of the calving front [*Howat et al.*, 2007; *Joughin et al.*, 2004; *Shuman et al.*, 2011; *Thomas*, 2004]. Thus, we compare the observed thinning with changes in calving front position and changes in ice flow speed. The

latter is obtained from measurements of ice motion by satellite interferometric synthetic-aperture radar (InSAR) data from the RADARSAT-1 satellite.

[7] Furthermore, to investigate potential triggers of these dynamically induced ice loss events, we analyze fluctuations in annual mean air and ocean temperatures.

2. Data Analysis

[8] Aerial photographs of UI were acquired on 23 July 1985, for the purpose of providing stereoscopic coverage of ice-free terrain including nunataks for topographic mapping. The available aerial photographs do not cover the entire catchment basin of Upernavik (see Figure 2). The scale is 1:150,000, and ground control, coordinate list, and image observations were provided by the Danish National Survey and Cadastre (http://www.kms.dk/Emner/Landkortogtopografi/ Groenland/Ground_control_Greenland.htm). The coordinates are in the GR96 reference system and mean sea level determined from the GR96 aero-analytical triangulation that uses geodetically surveyed stations for control. The heights are transformed to ellipsoid heights using the EGM96 geoid. The DEM is created from 34 photos, and the corresponding 277 ground control points from the coordinate list. We use these data to derive a 25×25 m gridded DEM for 1985 in a Universal Transverse Mercator reference system (zone 24) with elevations referenced to the height above the ellipsoid (World Geodetic System 1984 [WGS84]). Socet Set 5.5 (BAE Systems) and ArcGIS 10 (ESRI) were used to process the data.

[9] We evaluate the quality of the adjustment by examining a plot of the estimated mean errors on the heights (see Figure 2). These are found from the diagonal elements of the a posteriori covariance matrix resulting from the bundle block adjustment, and are determined by photo geometry and the arrangement of tie and ground control points, the
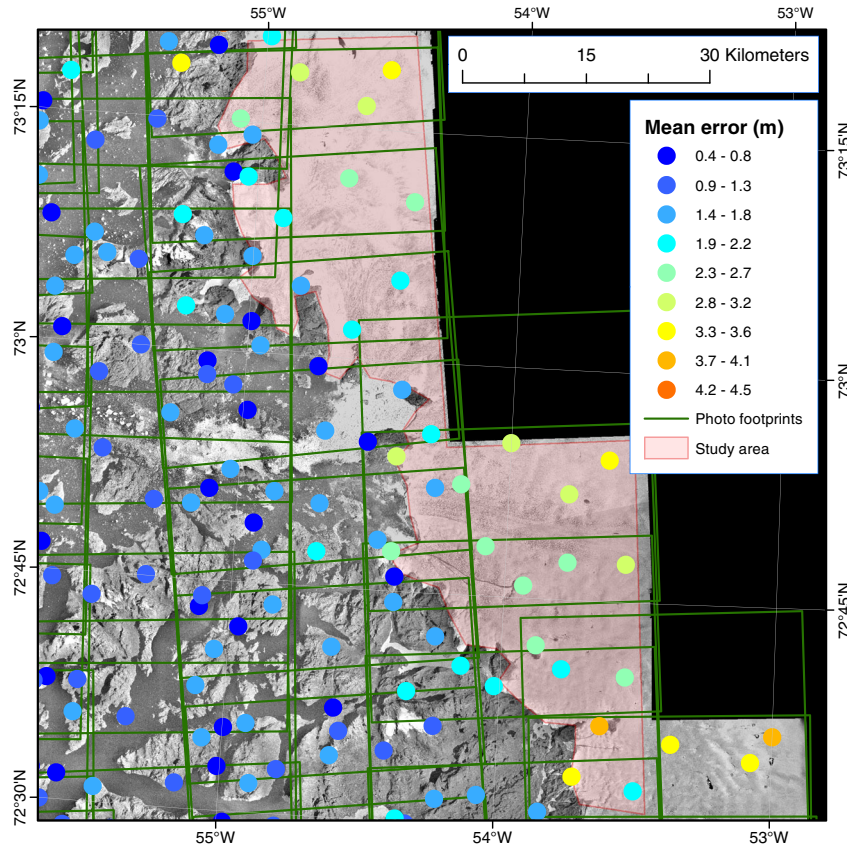
Figure 2. A posteriori mean error on heights determined from the bundle block adjustment. Mean errors for both ground control points (GCP) and tie points are shown. Green boxes denote photo footprints. Note the large sidelap of the photo footprints, which is by design. The large light red area denotes our study area.

latter two weighted for predicted errors. The mean value on the ice is 2.4 m (with a maximum value of 3.7 m and a minimum value of 1.3 m). For comparison, the values in the region between the ice-sheet margin and the outer coast have a mean of 1.3 m, a maximum of 4.1 m, and a minimum of 0.7 m. In the absence of checkpoints, we assess the accuracy of the 1985 DEM using 2002 to 2010 ATM data as reference data over ice-free terrain, including rocky outcrops in the ice. To obtain an assessment applicable to our modus of determining height change on the ice, we use only ATM heights with a corresponding measured and autocorrelated 1985 DEM height, resulting in 17,569 available sample points out of an initial 24,893. ATM data fulfill the requirement for this test by being at least an order of magnitude more accurate than the 1985 DEM data being evaluated. The resulting distribution and Gaussian fit for elevation differences on ice-free terrain suggest a standard deviation of $\sigma_{DEM85} = 3.8$ m. We assign each pixel in the 25 × 25 m grid an elevation uncertainty of 3.8 m. This number includes errors from the DEM generation, slope, andinterpolation, whereas the simulated mean errors do not. Previous validation studies using similar types of DEMs quoted an uncertainty of between 2.8 and 5.6 m [e.g., *Motyka et al.*, 2010].

[10] We use ICESat GLA12 Release 31 data [*Zwally et al.*, 2010] to resolve elevation changes relative to 1985. The Geoscience Laser Altimeter System instrument on ICESat provides measurements of ice-sheet elevations [*Zwally et al.*, 2010]. The ICESat elevations are provided relative to the TOPEX/Poseidon ellipsoid; we convert them to the WGS84 ellipsoid. The satellite laser footprint diameter is 30 to 70 m, and the distance between footprint centers is approximately 170 m.

[11] The dominant biases in ICESat elevations come from pointing errors, saturation errors, and atmospheric errors. However, pointing errors are now largely corrected in calibration [*Fricker et al.*, 2005; *Luthcke et al.*, 2005]. Signal saturation can cause heights to be biased low by up to 1.5 m [*Fricker et al.*, 2005]. Applying a saturation correction to the height reduces these errors (National Snow and Ice Data Center, available at http://nsidc.org/data/icesat/data_releases.html). A further bias can appear as prominent height anomalies that vary locally when clouds are present (− 0.16 m through thick cirrus) [*Zwally et al.*, 2010]. We use the difference between the shape of the return signal and a Gaussian fit (defined as the IceSvar parameter) to reject less reliable data. Large differences indicate less reliable surface elevation estimates. Measurements for which the misfit is large (IceSvar > 0.03) are rejected [*Smith et al.*, 2009]. Multiple peaks can be caused by cloud reflection. Waveforms that contain more than one peak in the return signal are also rejected from the analysis to remove additional bias from cloud reflection. The elevation accuracy depends on surface slopes. For ICESat elevations of flat surfaces that have been corrected for pointing errors and saturation errors, and that have been filtered for surface roughness and atmospheric scattering, the single-shot
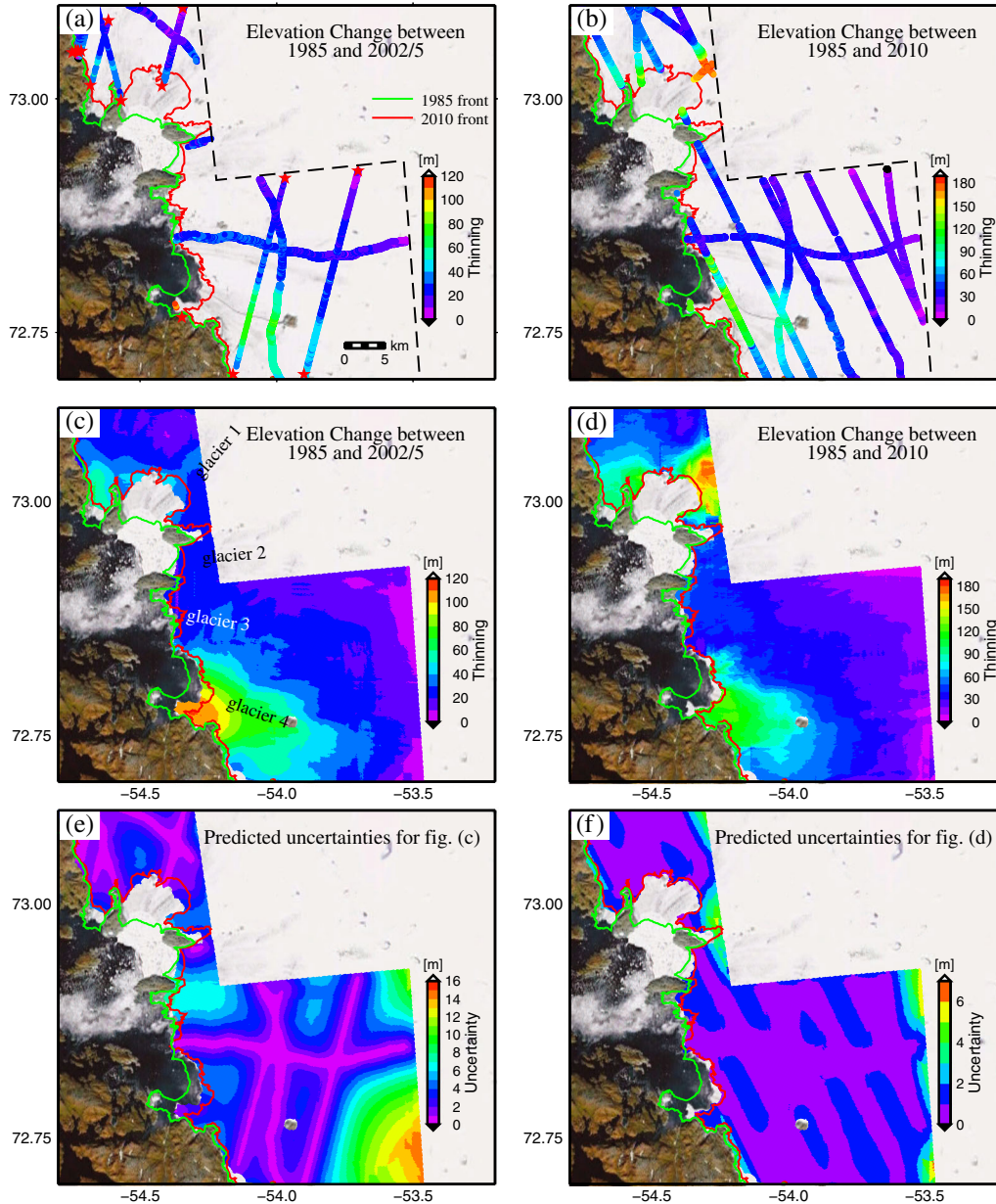
Figure 3. Colors indicate the change in elevation between 1985 and (a) 2002/2005 along the track line and (b) 2010 along the track line. Lines that start and end with red stars represent ICESat ground track lines, whereas all other lines represent ATM track lines. Note, no ICESat data are available for 2010. Dashed black lines at the eastern side of the map show areas not covered by the 1985 DEM. Color bar is in meters. Uncertainties are 3.8 m. Note, (a) uses a scale between 0 and 120 m, whereas (b) uses a scale between 0 and 190 m. (c and d) Interpolated thinning values (on a 25×25 m grid) between 1985 and 2002 to 2005, and between 1985 and 2010, respectively. (e and f) Predicted uncertainties for the interpolated thinning values shown in (c) and (d), respectively.

accuracy is $\sigma_{ICESat} = 0.2$ m [*Howat et al.*, 2008; *Pritchard et al.*, 2009; http://nsidc.org/data/icesat/data_releases.html]. As a complement to the ICESat data, we use ATM flight lines in this region for 2002, 2005, and 2010. The ATM measurements have an elevation accuracy of $\sigma_{ATM} = 0.1$ m [*Krabill et al.*, 2002].

[12] Furthermore, to detect catchment-wide ice loss, we use monthly gravity field solutions from the GRACE satellite gravity mission, generated by the Center for Space Research at the University of Texas, to estimate changes in

mass in the region surrounding UI between April 2002 and April 2012.

3. Results

3.1. Elevation Differences

[13] The Upernavik catchment basin (with an area of $\sim 22.5 \times 10^3$ km^2) is mostly drained through the four glaciers denoted by numbers 1 to 4 in Figure 1. To assess thinning before the recent acceleration (which started in mid-2005)
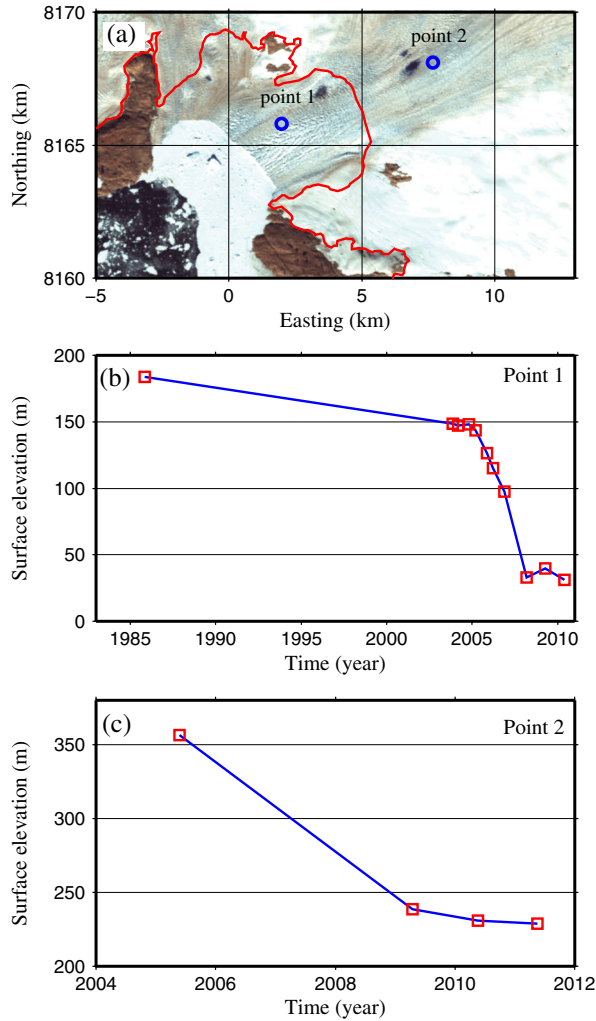
Figure 4. (a) Map of glacier 1 and locations of points 1 and 2. Red line denotes position of 2010 calving front. Landsat image is used as background. (b) Time series of elevations in meters at point 1 obtained using ATM, ICESat data, and 1985 DEM. (c) Same as (b), but for point 2.

we use ICESat and ATM data acquired between February and May in 2002, 2003, 2004, and 2005. ATM flight lines in this region between 1994 and 1999 cover only a single transect, located on glacier 3, and are therefore not used. As a compromise between having a reasonable spatial coverage over the region and a short time span, we use all available ATM and ICESat measurements acquired between 2002 and 2005 to quantify elevation changes before the recent acceleration in mid-2005.

[14] Figure 3a shows elevation differences for coastal UI between the 1985 DEM and 2002 and 2005-ATM track points, and between the 1985 DEM and 2003 and 2005 ICESat ground track points. The 1985 DEM does not cover the northeastern corner of the map, so no elevation change relative to 1985 is shown for that region. Figure 3b shows elevation differences between the 1985 DEM and 2010-ATM track points. (The ICESat mission stopped in 2009; consequently, no data for 2010 are available.) To estimate elevation change, we use ICESat and ATM track

points that are less than 17.8 m from the nearest 1985 DEM point (because the 1985 DEM grid spacing is 25 m; hence, the max distance to the nearest 1985 DEM point is $\sqrt{(0.5 \times 25)^2 + (0.5 \times 25)^2} = 17.8\ m$). Taking into account that ice surface is relatively flat and we use an uncertainty of 3.8 m, errors caused by the surface slope are small and can be ignored. The thinning values in Figure 3a and 3b have uncertainties of $\sigma_{thin} = \sqrt{\sigma_{DEM85}^2 + \sigma_{ATM}^2} = 3.8\ m$.

[15] Figure 3c shows interpolated thinning values (on a 25 × 25 m grid) between 1985 and 2002 to 2005. The interpolation is performed using the collocation method [*Heiskanen and Moritz*, 1967] and using the GRAVSOFT software package [*Forsberg and Tscherning*, 2008]. We use correlation distance of 25 km (the distance to where the covariance becomes half the variance). We use the observed thinning values (Figure 3a) with their associated uncertainty of 3.8 m to interpolate thinning values on a 25 × 25 m grid. For each grid point, we interpolate a thinning value dh_i^{interp} and estimate an associated uncertainty σ_i^{interp} [see *Heiskanen and Moritz*, 1967]. For the predicted thinning values shown in Figure 3c, we estimate a maximum uncertainty of 14.7 m (see Figure 3e). Similarly, Figure 3d shows interpolated elevation differences between 1985 and 2010. Here we estimate a maximum uncertainty of 6.2 m (see Figure 3f).

[16] The elevation differences between 1985 and 2002 to 2005 (Figure 3a) suggest that glacier 4 thinned much more than glaciers 1 to 3 during this time period. Glaciers 1 to 3 experienced widespread thinning on the order of 20 to 35 m, with maximum values near their calving fronts. The thinning along glacier 4 was much larger, with some of the track points thinning by as much as 111 ± 3.8 m on its southern tip.

[17] Figures 3b and 3d show elevation differences between 1985 and 2010. The results show increased thinning of glacier 1 (the maximum observed thinning rate on this glacier is 186 ± 3.8 m, near its calving front), but not much change in the elevations of glaciers 2 to 4 relative to 2002 through 2005.

[18] The implication from comparing Figure 3a with 3b (or 3c with 3d) is that glacier 4 underwent appreciable thinning of more than 100 m before 2002, whereas glacier 1 underwent appreciable thinning of more than 100 m after 2005. Glaciers 2 and 3 experienced widespread thinning during 1985 to 2010, but only on the order of 20 to 35 m.

[19] To further constrain the dynamically induced thinning on glacier 1, we use ATM, ICESat data, and the 1985 DEM to estimate a time series of surface elevation changes at two points (denoted as points 1 and 2 in Figure 4a) located near the front of glacier 1. At point 1 (Figure 4b), we observe thinning of approximately 30 m during 1985 to 2003 and no significant surface change during 2003 through 2005. Rapid thinning of more than 120 m starts in mid-2005 and lasts until summer 2007. In 2008, the glacier has retreated beyond point 1; hence, the observed surface elevation changes during 2008 to 2010 shown in Figure 4b represent the surface of floating icebergs in the fjord. Figure 4c shows surface elevation changes at point 2, which is located about 7 km farther upstream from point 1. Point 2 has fewer observations; however, it shows huge thinning of more than
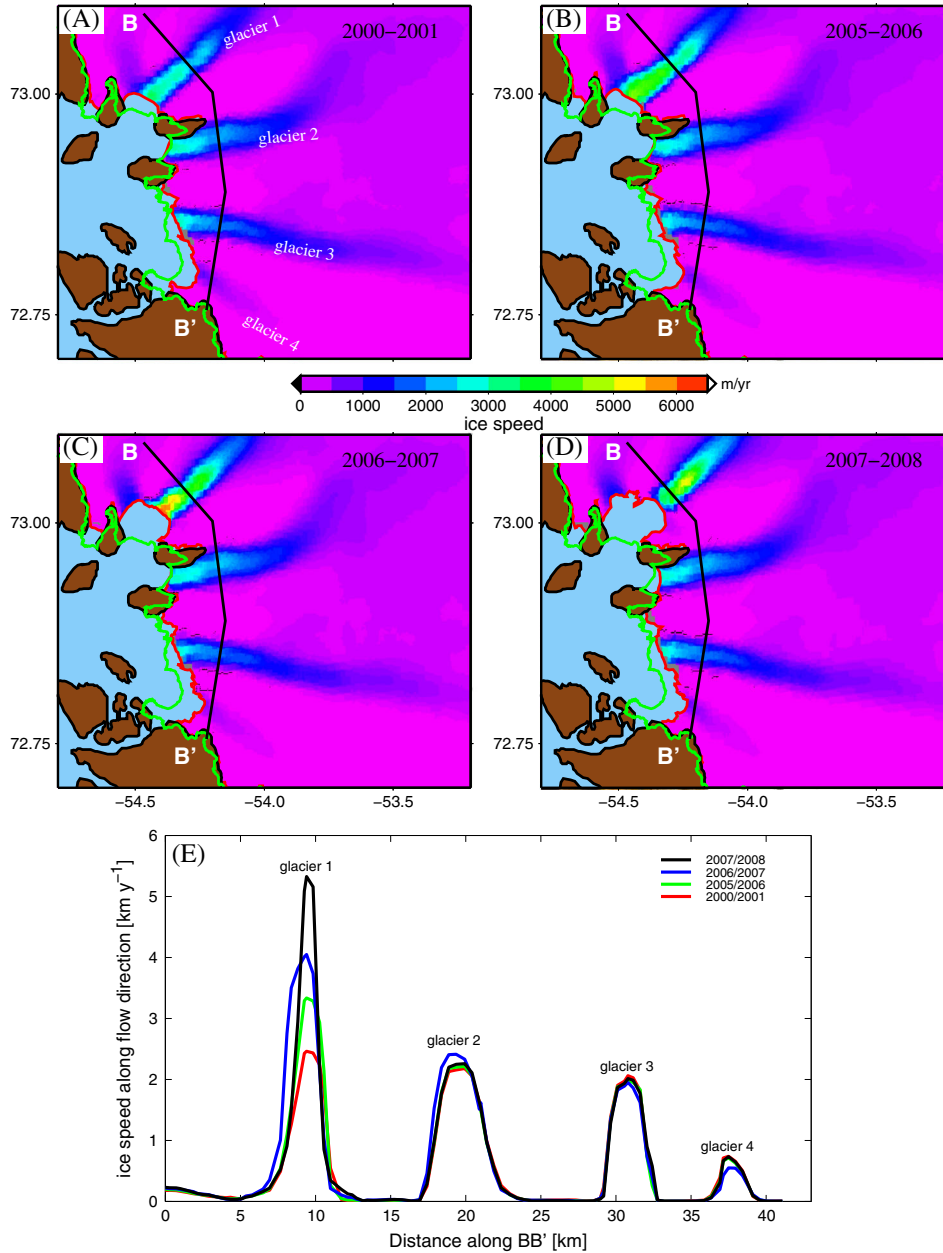
Figure 5. The winter ice speed obtained from measurements of ice motion by satellite InSAR data from the RADARSAT-1 satellite during (a) 2000 to 2001, (b) 2005 to 2006, (c) 2006 to 2007, and (d) 2007 to 2008. Colors indicate the speed. Color bar is in $m\,yr^{-1}$. (e) Ice speeds along the line BB' displayed in (a–d).

120 m during 2005 to 2009, and only 5 to 10 m during 2009 to 2011. The implication revealed by comparing Figure 4b with Figure 4c isthat the frontal portion of glacier 1 underwent huge dynamic thinning starting in mid-2005 and stabilized in summer 2009. Our results are consistent with observed surface elevation changes of glacier 1 by *McFadden et al.* [2011]. Their figure 4 (Upernavik North) shows thinning of 70 to 80 m during 2005 to 2006 of glacier 1.

3.2. Changes in Ice Speed

[20] To assess the dynamically induced thinning, we examine ice speeds along glaciers 1 to 4 during 2000 to 2008. We use winter velocity maps for Greenland, derived

using InSAR data from the RADARSAT-1 satellite, provided by the NSIDC [*Joughin et al.*, 2010]. Figure 5a shows winter ice speeds during 2000 to 2001. During this time period, glaciers 1 to 3 were moving at about $3.5\,km\,yr^{-1}$ near the calving front, with lower speeds farther inland (up-glacier). Figure 5b (the winter ice speed during 2005–2006) shows huge accelerations (>50% increase in the ice flow speed) near the front (<20 km) of glacier 1, whereas glaciers 2 to 4 show no significant changes in speed. The acceleration of the frontal portion of glacier 1 continued during 2006 to 2007 (Figure 5c) but slowed down during 2007 to 2008 (Figure 5d), whereas glaciers 2 to 4 remained stable. Figure 5d suggests the increased flow speeds of
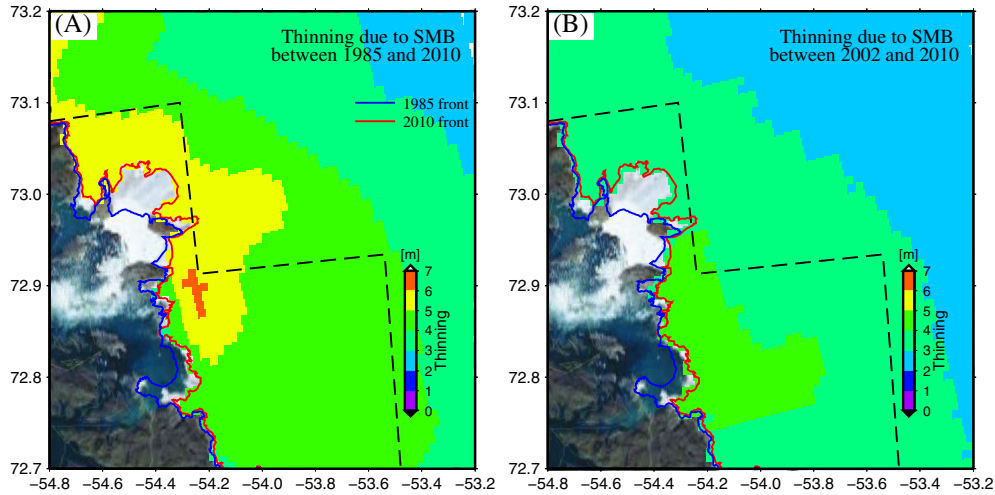
Figure 6. Total elevation change in meters caused by SMB fluctuations including firn compaction (a) between 1985 and 2010 and (b) between 2002 and 2010.

glacier 1 started migrating inland in 2007. Figure 5e shows glacier speeds along the line BB′ displayed in Figure 5a–d (solid black line). The line crosses all four glaciers and shows more than a 100% increase in the speed of glacier 1, but no notable acceleration (or deceleration) of glaciers 2 to 4. The NSIDC also provides uncertainty estimates related to the radar-derived velocity vectors [*Joughin et al.*, 2010]. The formal errors agree with errors determined by comparing radar-derived speeds with those derived from GPS data [*Joughin*, 2002]. The largest formal error along BB′ (provided by the NSIDC) is 0.1 km yr^{-1}, well below the observed speeds of glaciers 1 to 4 and change in speed at glacier 1.

3.3. SMB

[21] To isolate the dynamically induced thinning, we use the RACMO2, which is based on the high-resolution limited area model with physical processes adopted from the global model of the European Centre for Medium-Range Weather Forecasts (ECMWF). Its adaptation for the Greenland ice sheet, including the treatment of meltwater percolation and refreezing, as well as the evaluation of the modeled SMB, is described by *Ettema et al.* [2009] and *Ettema et al.* [2010]. The lateral boundary conditions are provided by ECMWF reanalyses, notably ERA-40 and ERA-Interim, and the model is run over the period from 1958 to 2010. Based on a comparison with observations, *Ettema et al.* [2009] concluded that the model performs very well (N = 265, r = 0.95), yielding a 14% uncertainty in ice-sheet integrated SMB; this is also the uncertainty we apply to the SMB of the individual glacier basins considered in this study. The elevation change shown in Figure 6 was derived from RACMO2 using SMB anomalies compared with the mean for 1961 through 1990, a period that shows no trend

in SMB [*van den Broeke et al.*, 2009]. Firn compaction and firn density were calculated using a model developed specifically for the percolation zone [*Reeh*, 2008]. Firn compaction has a negligible effect on the elevation change as the region lies within the ablation zone. The SMB anomaly was converted to an elevation change using the surface density from the model. Figure 6 shows total elevation change in meters caused by SMB fluctuations including firn compaction between 1985 and 2010 and between 2002 and 2010.

3.4. Ice-Volume Loss

3.4.1. Frontal Portion of UI

[22] We use the interpolated thinning values shown in Figure 3c and 3d and their associated uncertainties to estimate ice-volume change during 1985 to 2002/2005 and 1985 to 2010. For the frontal portion of UI that is covered by the 1985 DEM, we estimate a total ice-volume loss of $34.8 \pm 10.2 \, km^3$ between 1985 and 2002/2005, and $52.9 \pm 5.2 \, km^3$ during 1985 to 2010. The recent thinning and acceleration in ice speed is mainly caused by dynamic thinning on glacier 1. Because the 1985 DEM covers only the frontal approximately 5 km of glacier 1, the estimated ice-volume loss between 1985 and 2010 does not represent the total catchment-wide ice loss. Table 1 displays melt and dynamically induced ice-volume loss for the region covered by the 1985 DEM. The area of retreat during 1985 to 2010 is not included when computing the volume loss, and so the volume loss estimates listed in Table 1 are underestimated. To estimate melt-induced ice-volume loss, we use elevation changes caused by SMB fluctuations for the 1985 DEM region. Using an uncertainty of 14%, we estimate an ice-volume loss of $2.9 \pm 0.4 \, km^3$ between 1985 and 2002/2005, and $7.2 \pm 1.0 \, km^3$ during 1985 to 2010.

Table 1. Melt-Induced and Dynamically Induced Ice-Volume Change (in km^3) for the Region Covered by the 1985 DEM

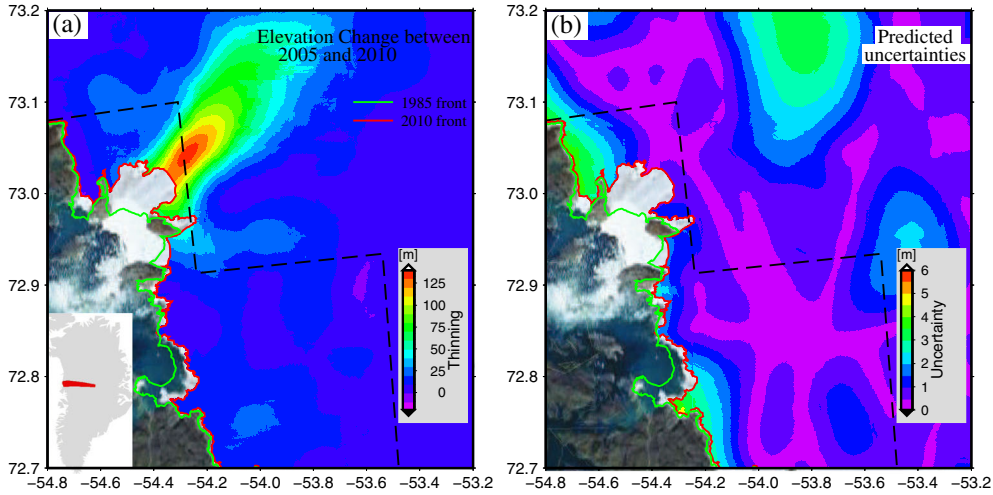|	1985–2002/2005	2002/2005–2010	1985–2010
Melt-induced ice loss	2.9 ± 0.5	4.5 ± 1.4	7.4 ± 1.3
Dynamically induced ice loss	31.9 ± 10.2	13.6 ± 11.5	45.5 ± 5.4
Total ice loss	34.8 ± 10.2	18.1 ± 11.4	52.9 ± 5.2

Figure 7. (a) Surface elevation changes during 2005 to 2010 and (b) their associated uncertainties in meters. Red line denotes position of 2010 calving front; blue line denotes position of 1985 calving front. Black dashed line denotes area covered by the 1985 DEM.

The dynamically induced ice-volume loss is obtained by subtracting melt-induced ice-volume loss from the observed ice-volume loss. To estimate ice-volume loss between 2002/2005 and 2010, we subtract the 1985 to 2002/2005 ice loss from the 1985 to 2010 ice loss.

3.4.2. UI Catchment Basin

[23] To estimate catchment-wide ice-volume loss of UI during 2005 to 2010, we use all available ICESat and ATM data supplemented with NASAâ€™s Land, Vegetation and Ice Sensor (LVIS) from 2010 [*Blair and Hofton*, 2010]. LVIS measurements have an elevation standard deviation of $\sigma_{LVIS} = 0.1$ m [*Blair and Hofton*, 2010]. To derive ice-surface change estimates, we first divide the entire UI drainage basin into 500 ± 500 m cells. We assume the ice surface of cell (i,j) includes a seasonal term and a secular term. Thus, the observed height H_{ij} of the (i,j)'th cell at time t can be expressed as:

$$H_{ij}(t) = a_{ij}t + b_{ij} + \alpha_{ij}\cos(\omega t) + \beta_{ij}\sin(\omega t) + SE_{ij}\left(E - E_{ij}^0\right)$$
$$+ SN_{ij}\left(N - N_{ij}^0\right), \tag{1}$$

where a_{ij} represents the secular term and b_{ij} an offset. The seasonal term is described by the α_{ij} and β_{ij},

$$A_{ij}\cos\left(\omega t + \varphi_{ij}\right) = \alpha_{ij}\cos(\omega t) + \beta_{ij}\sin(\omega t), \tag{2}$$

where ω is the frequency of the annual term, and A_{ij} and φ_{ij} are the amplitude and phase of the annual term, respectively. $(E - E_{ij}^0)$ and $(N - N_{ij}^0)$ are the Easting and Northing observations relative to the nominal cell center coordinates E_{ij}^0 and N_{ij}^0 of the (i,j)'th cell. SE_{ij} is the ice slope of the (i,j)'th cell in the eastern direction, whereas NE_{ij} is the ice slope of the (i,j)'th cell in the northern direction.

$$SE_{ij} = \left(\frac{dH}{dE}\right)_{ij}, SN_{ij} = \left(\frac{dH}{dN}\right)_{ij}. \tag{3}$$

[24] Our procedure for deriving ice-surface elevation changes is similar to the method used by, for example, *Ewert et al.* [2012], *Howat et al.* [2008], and *Smith et al.* [2009].

For each (i,j)'th cell point in the UI drainage basin, we search for all available ICESat, ATM, and LVIS data points located within the cell. Thus, we find all data points within the 500×500 m box and simultaneously fit (using least squares) annually and secularly varying terms, and slopes in the easterly and northerly directions. Next, we use the observed ice-elevation change rates with their associated uncertainties to interpolate (using collocation) ice-thinning values onto a regular grid.

[25] Figure 7a and 7b show ice elevation changes during 2005 to 2010 and their associated uncertainties, respectively. Figure 7 show huge thinning (>100 m) on glacier 1, and only minor thinning (10–25 m) on glaciers 2 to 4. The UI catchment basin extends about 450 km inland (see lower left panel in Figure 7a) and corresponds to area 24 of *Rignot and Kanagaratnam* [2006]. Table 2 displays catchment-wide dynamically and melt-induced ice-mass loss during 2005 to 2010. To convert ice volume to mass, we use the simple firn compaction model of *Reeh*, [2008]. We estimate a total mass loss of 53.5 ± 12.8 Gt during 2005 to 2010, where the contribution of dynamically induced mass loss is 80% (43.0 ± 12.9 Gt).

3.5. Catchment-Wide Ice Loss From GRACE

[26] To detect catchment-wide ice loss, we use gravity field solutions from the GRACE satellite gravity mission to estimate changes in mass in the region surrounding UI between April 2002 and April 2012. In brief, we use monthly, Release-4 gravity fields in the form of spherical harmonic (Stokes) coefficients, generated at the Center for Space Research at the University of Texas. We augment those fields by replacing the GRACE C20 values with C20

Table 2. Melt-Induced and Dynamically Induced Mass Loss (in Gigatons) During 2005–2010 for the UI Catchment Basin

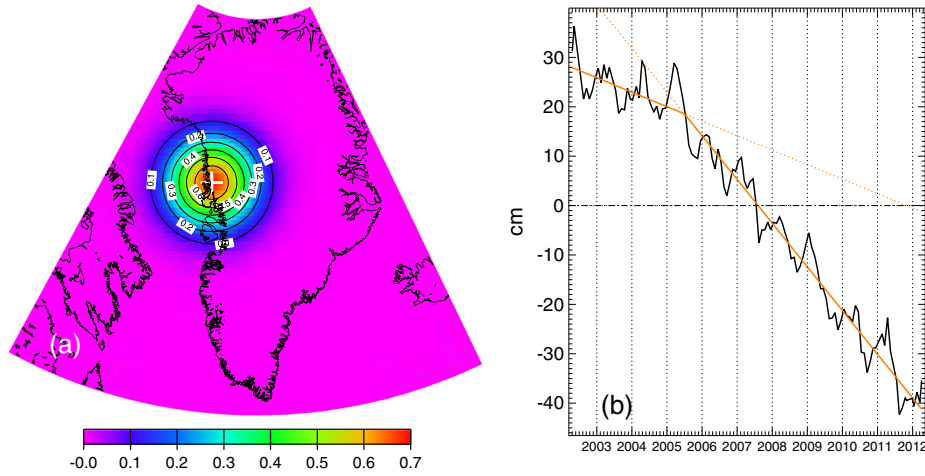|	
Melt-induced mass loss	10.5 ± 1.5 Gt
Dynamically induced mass loss	43.0 ± 12.9 Gt
Total mass loss	53.5 ± 12.8 Gt

Figure 8. (a) The GRACE averaging function; a Gaussian with a 250 km half width, centered at the location of the white plus sign, which is at the UI calving front. (b) The GRACE time series of surface mass, in centimeters of water thickness, computed using the averaging function shown in (a). The two solid orange lines denote the best-fitting straight lines before and after 1 July 2005. The dashed orange lines, which are extensions of those best-fitting lines, help to illustrate the increase in mass loss that began in mid-2005.

values obtained using satellite laser ranging [*Cheng et al.*, 2011], and including degree-one terms computed from GRACE data as described by *Swenson et al.* [2008]. We remove contributions from global water storage outside Greenland, using the Global Land Data Assimilation System (GLDAS)/Noah land surface model [*Rodell et al.*, 2004], and we redistribute any net global mass loss or gain predicted by GLDAS into the ocean. We correct for glacial isostatic adjustment (GIA) by removing model results based on the global ICE-5 G deglaciation history and VM2 viscosity profile [*Peltier*, 2004], computed as described in *A et al.* [2012]. We apply the decorrelation filter described by *Swenson and Wahr* [2006] to the GRACE-minus-GLDAS-minus-GIA Stokes coefficients. Finally, we construct a monthly time series from the filtered results, by computing a Gaussian average with a 250 half width [*Wahr et al.*, 1998] about a point close to the UI calving front.

[27] The 250 km Gaussian averaging function is shown in Figure 8a, to illustrate the sensitivity of our GRACE estimates to mass loss in the region surrounding UI. Our monthly time series is shown in Figure 8b. There is a clear increase in the rate of mass loss in mid-2005, as illustrated by the difference in slopes between the two solid, best-fitting orange lines.

3.6. Sea Surface and Air Temperatures

[28] To investigate potential triggers for the dynamically induced thinning on glaciers 1 and 4, we analyze sea-surface temperature (SST) and air temperatures. Figure 9a shows mean annual SST anomalies in degrees Celsius between 1981 and 2011 at three locations along the northwest coast of Greenland. SST data were obtained from the Met Office Hadley Centre observation data sets (http://www.metoffice.gov.uk/hadobs/hadisst/data/download.html). The SST anomalies show relatively warm temperatures in the mid- and late-1980s and during the 2000s. Figure 9b shows mean annual air temperatures in degrees Celsius (after removing the 1981–2010 mean) at Upernavik, obtained from the Danish

Meteorological Institute. Similar to the SST anomalies, the air temperatures show high values during the 2000s and 1980s. Hence, the high air temperature and SST in the 1980s could potentially have triggered the pre-2000 retreat of glacier 4 (and thinning before 2002). Similarly, the observed frontal retreat, speedup, and thinning on glacier 1
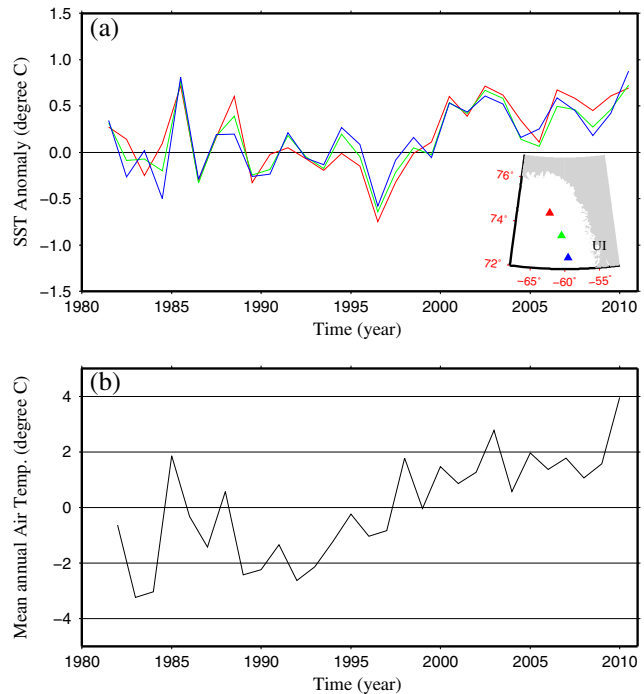

Figure 9. (a) Mean annual SST anomaly in degrees Celsius between 1981 and 2011 at three locations along the northwest coast of Greenland obtained from the Met Office Hadley Centre observations data sets. (b) Mean annual air temperature in degrees Celsius (after removing the 1981–2010 mean) at Upernavik obtained from the Danish Meteorological Institute.

was potentially triggered by a combination of increased air and ocean temperatures.

4. Discussion and Conclusions

[29] The rapid increase in glacier ice speeds seen in many places has been attributed to decreased flow resistance and increased along-flow tensile stresses during the retreat of the calving front [*Howat et al.*, 2007; *Joughin et al.*, 2004; *Shuman et al.*, 2011; *Thomas*, 2004]. The observed speedup of glacier 1 in 2005 to 2006 (Figure 5) coincides with decreased flow resistance as the calving front retreats (Figure 1). The calving front of glacier 1 appeared stable during 1985 to 1996. It retreated by approximately 1 km during 1996 to 2000, approximately 1 km during 2000 to 2005, and about 5 km during 2005 to 2008 (see Figure 1), but appeared relatively stable during 2008 to 2010. The calving fronts of glaciers 2 and 3 appeared relatively stable (retreated by 1–2 km) during the entire 1985 to 2010 time period. The calving front of glacier 4 retreated by approximately 2 km between 1985 and 1991, and approximately 1 km between 1996 and 2000 (Figure 1), but appeared relatively stable during 2000 to 2010.

[30] Measurements of the surface elevation along ICESat and ATM track points differenced with the 1985 DEM suggest large-scale thinning (>100 m during 1985–2010) on glaciers 1 and 4. However, Figures 3 and 4 suggests rapid thinning on glacier 1 starting in summer 2005, whereas thinning on glacier 4 occurred before 1991 (based on the 1985–1991 retreat of the calving front). The timing of the glacier 1 thinning is consistent with the observed speedup on several glaciers along the northwest coast of Greenland [*Joughin et al.*, 2010; *Pritchard et al.*, 2009] and the mass loss observed using GRACE satellite data [*Khan et al.*, 2010].

[31] Figures 3 to 6 suggest that the thinning by tens of meters on glacier 1 is dynamically induced. The timing of that thinning coincides with the observed greater than 50% increase in the flow speed of glacier 1 during 2005 to 2006 relative to 2000 to 2001. SMB data suggest 4 to 6 m of melt-induced thinning during 1985 to 2010 on glaciers 1 to 4 (Figure 6). Thus, some of the observed thinning of 15 to 30 m during 1985 to 2010 on glaciers 1 to 4 can be explained as melt-induced thinning. Because glaciers 3 and 4 are located only about 10 km apart, the melt-induced thinning should be similar for the two glaciers; the SMB results suggest elevation change differences of less than 1 m (Figure 6). Consequently, the relatively large thinning of glacier 4 is most plausibly explained as dynamic thinning.

[32] Our observations show dynamically induced ice-volume loss on the frontal portion of UI of $45.5 \pm 5.4 \, \mathrm{km^3}$ (during 1985–2010), whereas the total melt-induced ice-volume loss during this same period is $7.4 \pm 1.3 \, \mathrm{km^3}$. Ice loss took place on different glaciers and during different time intervals. The first period of ice loss is associated with huge thinning (>100 m) on glacier 4 and only minor thinning on glaciers 1 to 3. The second period of ice loss is associated with huge thinning on glacier 1 and only minor thinning on glaciers 2 to 4. UI appears to be thinning and retreating stepwise, and the thinning and retreat do not always take place on the same glacier.

[33] In this article, we have documented at least two periods of ice loss characterized by a retreat of the calving front, increased ice speeds, and thinning. The most recent ice loss coincides with speedup on several glaciers along the northwest coast of Greenland [*Pritchard et al.*, 2009; *Joughin et al.*, 2010] and mass loss observed using GRACE satellite data (Figure 8). *Kjær et al.* [2012] recently reported dynamically induced ice-loss events on the northwestern Greenland Ice Sheet margin from 1985 to 1993 and 2005 to 2010. The first event observed here (on glacier 4) could possibly have taken place during 1985 to 1991 and been triggered by relatively high ocean and air temperatures.

[34] Our observations show that dynamically induced accelerations of ice loss last until the glacier stabilizes; for example, glacier 4 experienced dynamically induced accelerations of ice loss before 2002, but we observe no significant dynamically induced thinning on that glacier during 2002 to 2010 (and no significant retreat of the front during 1991–2010). Similar observations have been made in southeast Greenland where rapid speedup of ice flow and retreat in 2003 to 2004 [*Howat et al.*, 2005; *Stearns and Hamilton*, 2007] was followed by a deceleration [*Howat et al.*, 2008] and stabilization in 2006 [*Nick et al.*, 2009]. Consequently, extrapolation of future ice loss from the recent dynamically induced acceleration of ice loss in Greenland's outlet glaciers should be done with caution.

[35] We estimate catchment-wide dynamically induced mass loss of 43.0 ± 12.9 Gt during 2005 to 2010 (Table 2), which is about 80% of the total ice loss. By converting the volume listed in Table 1 to mass, we obtain a dynamically induced mass loss of 29.3 ± 9.2 Gt during 1985 to 2002. Taking into account that this is a minimum mass loss rate because the area of retreat is not included when computing the volume loss, we estimate a minimum catchment-wide, dynamically induced mass loss of 72.3 ± 15.8 Gt during 1985 to 2010. Catchment-wide melt-induced mass loss for the same period is 19.8 ± 2.8 Gt. Hence, the UI catchment basin lost a total of at least 92 ± 15.8 Gt during 1985 to 2010, where at least 79% was due to dynamic thinning. This indicates the importance of including dynamically induced ice loss in the total mass change budget of the Greenland ice sheet.

[36] However, it should be noted that our ratio between melt and dynamically induced ice loss is probably not representative of the entire northwest Greenland ice sheet, because other glaciers along the northwest coast experienced less dynamic thinning [*Kjær et al.*, 2012; *McFadden et al.*, 2011], and so their relative contributions from dynamic ice loss are expected to be smaller.

References

A, G., J. Wahr, and S. Zhong (2012), Computations of the viscoelastic response of a 3-D compressible Earth to surface loading: An application to Glacial Isostatic Adjustment in Antarctica and Canada, *Geophys. J. Int.*, doi: 10.1093/gji/ggs030, in press.

Blair, B., and M. Hofton (2010), IceBridge LVIS L2 Geolocated Ground Elevation and Return Energy Quartiles, NASA Distributed Active Archive

Center at the National Snow and Ice Data Center, Boulder, Colo., http://nsidc.org/data/ilvis2.html.

Chen, J. L., C. R. Wilson, and B. D. Tapley (2006), Satellite gravity measurements confirm accelerated melting of Greenland ice sheet, *Science*, *313*, 1958–1960, doi:10.1126/science.1129007.

Cheng, M., J. C. Ries, and B. D. Tapley (2011), Variations of the Earth's figure axis from satellite laser ranging and GRACE, *J. Geophys. Res.*, *116*, B01409, doi:10.1029/2010JB000850.

Ettema, J., M. R. van den Broeke, E. van Meijgaard, W. J. van de Berg, J. L. Bamber, J. E. Box, and R. C. Bales (2009), Higher surface mass balance of the Greenland ice sheet revealed by high-resolution climate modeling, *Geophys. Res. Lett.*, *36*, L12501, doi:10.61029/2009GL038110.

Ettema, J., M. R. van den Broeke, E. van Meijgaard, W. J. van de Berg, J. E. Box, and K. Steffen (2010), Climate of the Greenland ice sheet using a high-resolution climate model. Part 1: Evaluation, *The Cryosphere*, *4*, 511–527.

Ewert, H., A. Groh, and R. Dietrich (2012), Volume and mass changes of the Greenland ice sheet inferred from ICESat 203 and GRACE, *J. Geodyn.*, *59–60*, 111–123, doi:10.1016/j.jog.2011.06.003.

Forsberg, R., and C. C. Tscherning (2008), An Overview Manual for the GRAVSOFT, Geodetic Gravity Field Modelling Programs, 2nd ed., Niels Bohr Institute, University of Copenhagen, Copenhagen, Denmark.

Fricker, H. A., A. Borsa, B. Minster, C. Carabajal, K. Quinn, and B. Bills (2005), Assessment of ICESat performance at the salar de Uyuni, Bolivia, *Geophys. Res. Lett.*, *32*, L21S06, doi:10.1029/2005GL023423.

Heiskanen, W. A., and H. Moritz (1967), Physical Geodesy, 364 pp., W.H. Freeman, San Francisco.

Howat, I. M., I. Joughin, S. Tulaczyk, and S. Gogineni (2005), Rapid retreat and acceleration of Helheim Glacier, east Greenland, *Geophys. Res. Lett.*, *32*, L22502, doi:10.1029/2005GL024737.

Howat, I. M., I. Joughin, and T. A. Scambos (2007), Rapid changes in ice discharge from Greenland outlet glaciers, *Science*, *315*, 1559, doi:10.1126/science.1138478.

Howat, I. M., B. E. Smith, I. Joughin, and T. A. Scambos (2008), Rates of southeast Greenland ice volume loss from combined ICESat and ASTER observations, *Geophys. Res. Lett.*, *35*, L17505, doi:10.1029/2008GL034496.

Joughin, I. (2002), Ice-sheet velocity mapping: A combined interferometric and speckle-tracking approach, *Ann. Glaciol.*, *34*, 195–201. doi:10.3189/172756402781817978.

Joughin, I., B. Smith, I. M. Howat, T. Scambos, and T. Moon (2010), Greenland flow variability from ice-sheet-wide velocity mapping, *J. Glaciol.*, *56*(197), 415–430.

Joughin, I., W. Abdalati, and M. Fahnestock (2004), Large fluctuations in speed on Greenland's Jakobshavn glacier, *Nature*, *432*, 608–610, doi:10.1038/nature03130.

Joughin, I., I. M. Howat, M. Fahnestock, B. Smith, W. Krabill, R. B. Alley, H. Stern, and M. Truffer (2008), Continued evolution of Jakobshavn Isbræ following its rapid speedup, *J. Geophys. Res.*, *113*, F04006, doi:10.1029/2008JF001023.

Khan, S. A., J. Wahr, L. A. Stearns, G. S. Hamilton, T. van Dam, K. M. Larson, and O. Francis (2007), Elastic uplift in southeast Greenland due to rapid ice mass loss, *Geophys. Res. Lett.*, *34*, L21701, doi:10.1029/2007GL031468.

Khan, S. A., J. Wahr, M. Bevis, I. Velicogna, and E. Kendrick (2010), The spread of ice mass loss into northwest Greenland observed by GRACE and GPS, *Geophys. Res. Lett.*, *37*, L06501, doi:10.1029/2010GL042460.

Kjær, K. H., et al. (2012), Aerial photographs reveal late-20th-century dynamic ice loss in Northwestern Greenland, *Science*, *337*, 569, doi:10.1126/science.1220614.

Krabill, W. B. (2011), IceBridge ATM L2 Icessn Elevation, Slope, and Roughness, [1994-2010], National Snow and Ice Data Center, Boulder, Colo.

Krabill, W. B., W. Abdalati, E. B. Frederick, S. S. Manizade, C. F. Martin, J. G. Sonntag, R. N. Swift, R. H. Thomas, and J. G. Yungel (2002), Aircraft laser altimetry measurement of elevation changes of the Greenland ice sheet: Technique and accuracy assessment, *J. Geodyn.*, *34*, 357–376, doi:10.1016/S0264-3707(02)00040-6.

Krabill, W. B., et al. (2004), Greenland ice sheet: Increased coastal thinning, *Geophys. Res. Lett.*, *31*, L24402, doi:10.1029/2004GL021533.

Lemke, P., et al. (2007), Observations: Changes in snow, ice and frozen ground, in Climate Change 2007: The Physical Science Basis. Contribution of Working Group I to the Fourth Assessment Report of the Intergovernmental Panel on Climate Change, pp. 361–369, Cambridge University Press, Cambridge, United Kingdom.

Liu, L., J. Wahr, I. Howat, S. A. Khan, I. Joughin, and M. Furuya (2012), Constraining ice mass loss from Jakobshavn Isbræ (Greenland) using InSAR-measured crustal uplift, *Geophys. J. Int.*, *188*, 994–1006, doi:10.1111/j.1365-246X.2011.05317.x.

Luthcke, S. B., D. D. Rowlands, T. A. Williams, and M. Sirota (2005), Calibration and reduction of ICESat geolocation errors and the impact on ice sheet elevation change detection, *Geophys. Res. Lett.*, *32*, L21S05, doi:10.1029/2005GL023689.

Luckman, A., T. Murray, R. de Lange, and E. Hanna (2006), Rapid and synchronous ice-dynamic changes in East Greenland, *Geophys. Res. Lett.*, *33*, L03503, doi:10.1029/2005GL025428.

McFadden, E. M., I. M. Howat, I. Joughin, B. E. Smith, and Y. Ahn (2011), Changes in the dynamics of marine terminating outlet glaciers in west Greenland (2000-2009), *J. Geophys. Res.*, *116*, F02022, doi:10.1029/2010JF001757.

Motyka, R. J., M. Fahnestock, and M. Truffer (2010), Volume change of Jakobshavn Isbræ, West Greenland: 1985-1997-2007, *J. Glaciol.*, *56*, 198.

Nick, N. M., A. Vieli, I. M. Howat, and I. Joughin (2009), Large-scale changes in Greenland outlet glacier dynamics triggered at the terminus, *Nat. Geosci.*, *2*, 110–114, doi:10.1038/NGEO394.

Nielsen, K., S. A. Khan, N. J. Korsgaard, K. H. Kjær, J. Wahr, M. Bevis, L. Stearns, and L. H. Timm (2012), Recent changes on Upernavik Isstrøm, West Greenland, *Earth Planet. Sci. Lett.*, *353-354*, 182–189, doi:10.1016/j.epsl.2012.08.024.

Peltier, W. R. R. (2004), Global glacial isostasy and the surface of the Ice-Age Earth: The ICE-5G (VM2) model and GRACE, *Annu. Rev. Earth Planet. Sci.*, *32*(1), 111–149, doi:10.1146/annurev.earth.32.082503.144359.

Pritchard, H. D., R. J. Arthern, D. G. Vaughan, and L. A. Edwards (2009), Extensive dynamic thinning on the margins of the Greenland and Antarctic ice sheets, *Nat. Geosci.*, *461*, 971–975, doi:10.1038/nature08471.

Reeh, N. (2008), A nonsteady-state firn-densification model for the percolation zone of a glacier, *J. Geophys. Res.*, *113*, F03023, doi:10.1029/2007JF000746.

Rignot, E., and P. Kanagaratnam (2006), Changes in the velocity structure of the Greenland ice sheet, *Science*, *311*, 986–990, doi:10.1126/science.1121381.

Rodell, M., et al. (2004). The Global Land Data Assimilation System, *Bull. Am. Meteorol. Soc.*, *85*(3), 381–394, doi:310.1175/BAMS-1185-1173-1381.

Shuman, C. A., E. Berthier, and T. A. Scambos (2011), 2001–2009 elevation and mass losses in the Larsen A and B embayments Antarctic Peninsula, *J. Glaciol.*, *57*(204), 737–754.

Smith, B. E., H. A. Fricker, I. R. Joughin, and S. Tulaczyk (2009), An inventory of active subglacial lakes in Antarctica detected by ICESat (2003–2008), *J. Glaciol.*, *55*, L21S09, doi:10.3189/002214309789470879.

Stearns, L. A., and G. S. Hamilton (2007), Rapid volume loss from East Greenland outlet glaciers quantified using repeat stereo satellite imagery, *Geophys. Res. Lett.*, *34*, L05503, doi:10.1029/2006GL028982.

Swenson, S., and J. Wahr (2006), Post-processing removal of correlated errors in GRACE data, *Geophys. Res. Lett.*, *33*, L08402, doi:10.1029/2005GL025285.

Swenson, S., D. Chambers, and J. Wahr (2008), Estimating geocenter variations from a combination of GRACE and ocean model output, *J. Geophys. Res.*, *113*, B08410, doi:10.1029/2007JB005338.

Thomas, R. H. (2004), Force-perturbation analysis of recent thinning and acceleration of Jakobshavn Isbræ, Greenland, *J. Glaciol.*, *50*(168), 57–66, doi:10.3189/172756504781830321.

van den Broeke, M., J. Bamber, J. Ettema, E. Rignot, E. Schrama, W. J. van de Berg, E. van Meijgaard, I. Velicogna, and B. Wouters (2009), Partitioning recent Greenland mass soss, *Science*, *326*, 984, doi:10.1126/science.1178176.

Velicogna, I. (2009), Increasing rates of ice mass loss from the Greenland and Antarctic ice sheets revealed by GRACE, *Geophys. Res. Lett.*, *36*, L19503, doi:10.1029/2009GL040222.

Wahr, J., M. Molenaar, and F. Bryan (1998), Time variability of the Earth's gravity field: Hydrological and oceanic effects and their possible detection using GRACE, *J. Geophys. Res.*, *103*(12), 30205–30229.

Zwally, H. J., R. Schutz, C. Bentley, J. Bufton, T. Herring, J. Minster, J. Spinhirne, and R. Thomas (2010), GLAS/ICESat L2 Antarctic and Greenland Ice Sheet Altimetry Data V031, National Snow and Ice Data Center, Boulder, Colo.